Harmonic active mode locking in terahertz quantum cascade lasers

Carlo Silvestri [●],[1] Xiaoqiong Qi,[1] Thomas Taimre [●],[2] and Aleksandar D. Rakić [●][1]

[1]*School of Information Technology and Electrical Engineering, University of Queensland, Brisbane, Queensland 4072, Australia*
[2]*School of Mathematics and Physics, University of Queensland, Brisbane, Queensland 4072, Australia*

We present a numerical study of the active harmonic mode locking (HML) of quantum cascade lasers (QCLs) in the terahertz (THz) spectral range. This is a recently experimentally demonstrated technique based on the modulation of the bias current of the laser by radio-frequency (rf) injection, allowing for the generation of multiple short pulses per round-trip in the QCL cavity. We first study the Fabry-Pérot (FP) configuration, unraveling the impact of both laser intrinsic parameters and rf injection on the characteristics of the generated harmonic pulses. Our study demonstrates that the key parameter for the achievement of ultrashort pulses is the QCL gain bandwidth: by pushing this quantity beyond 1 THz, we reproduce second-order ultrashort harmonic pulses with a duration of 2.5 ps. This suggests that the combination of the HML technique with the design of optimized cavities providing a larger gain, such as multistack active regions, can allow for the generation of narrow pulses approaching the picosecond limit in THz QCLs. Then a direct comparison with the experiment is presented, which reveals that the introduction of an unmodulated section in the laser cavity is crucial to considerably reduce the duration of the generated pulses. Finally, motivated by recent observations of high-contrast localized structures such as optical solitons in free-running ring QCLs, we investigate the formation of harmonic pulses in these unidirectional cavities. We make a comparative analysis aimed at understanding if this configuration can guarantee an improvement in the performance of the HML with respect to the FP case. We find that the intrinsic properties of ring QCLs, such as unidirectionality and the absence of spatial hole burning, lead to a 1.5-ps pulse duration, promoting these devices as strong candidates for the generation of ultrashort pulses in the THz range.

I. INTRODUCTION

Quantum cascade lasers (QCLs) are semiconductor lasers based on intraband transitions occurring between confined states in the conduction band of heterostructures made of narrow (thickness on the nanometer scale) layers of semiconductor materials [1]. They are, therefore, unipolar devices. The emission wavelength and all the characteristics of these lasers can be chosen by performing band-gap engineering and, for this reason, emission in spectral ranges not covered by conventional bipolar semiconductor lasers is achieved. Quantum cascade lasers were first demonstrated in the mid-infrared (mid-IR) spectral region [2] and then in the terahertz (THz) range [3], where they represent the only compact light source emitting high power [4]. In the past decade, the study of the multimode emission of THz QCLs has experienced a rapid development, with the experimental observation and characterization of self-generated optical frequency combs (OFCs) [5], coherent regimes which can be exploited for important applications in the imaging, communication, and spectroscopic domains [4,6–9]. More recently, the demonstration of harmonic frequency combs in the THz range has been achieved, with the observation of spontaneous formation of multimode regimes characterized by equally spaced optical lines with the spacing of a multiple of the free-spectral range (FSR) of the QCL cavity [10–13]. Moreover, it has been shown recently that in a long-cavity THz QCL the free-running harmonic pulsations of the density or carriers result in more stability

than the fundamental pulses [14]. In both mid-IR and THz ranges, the spontaneous OFCs are characterized by the coexistence of amplitude modulated (AM) and frequency modulated behavior, as outlined by theoretical [15–24] and experimental [5,25–28] works, and therefore present different properties when compared with the regimes obtained by performing an active mode locking of the laser. The fundamental active mode locking of QCLs in the THz region has been implemented by modulating the bias current of the laser by radio-frequency (rf) injection. In this case high-contrast regular pulses characterized by AM behavior are generated and occur on the timescale of the round-trip frequency of the laser cavity [29–33]. A challenging problem related to the generation of these QCL pulses is the development of strategies to increase their repetition rate and decrease their width, with the long-standing goal to achieve a pulse duration of 1 ps or lower, in the THz range. Active harmonic mode locking (HML) constitutes a possible solution for this problem. This technique is based on the modulation of the bias current with a frequency which is a multiple of the beat-note (BN) frequency of the laser. In this way, depending on the order of the HML, multiple times faster coherent operation of the laser is actively induced, with the generation of pulses with repetition frequency which is a multiple of the round-trip frequency of the QCL. Recently, the first experimental demonstration of active HML of THz QCLs has been reported [12,13], paving the way for promising potential applications in high bit-rate THz communication and photonic generation of microwaves at high frequencies [12].

In this experiment a Fabry-Pérot (FP) QCL was employed for the generation of second-order harmonic pulses, characterized by a measured duration of 25 ps. However, no further experiment and no systematic theoretical study on this method have been presented so far. This motivates the theoretical analysis presented in this work, aimed to outline the ideal configuration for the implementation of the active HML and provide guidance for future experiments. For this purpose, we adopt the effective semiconductor Maxwell-Bloch equations (ESMBEs) [16,17,34], a theoretical model which encompasses the main features of the interaction between the light and the active medium of a QCL.

The first part of the work is dedicated to the FP configuration. We initially adopt convenient values for the ESMBE parameters that allow one to reproduce with reasonable agreement the main experimental observations on spontaneous generation of frequency combs and fundamental active mode locking in THz QCLs and that also enable the reproduction of harmonic regimes by modulating the driving current [16]. Using this as a starting point, we investigate the influence of the intrinsic laser characteristics, tuning α factor, gain bandwidth, carrier lifetime, and the impact of the rf injection parameters on the characteristics of the HML in FP THz QCLs. This analysis leads to a convenient optimization of the HML performance, with the numerical reproduction of second-order harmonic pulses with a duration of 2.5 ps.

Furthermore, we simulate the configuration exploited in [12], establishing a direct comparison with the experiment and highlighting possible strategies to reduce the pulse duration. We find out that the introduction of an unmodulated section in the FP cavity is crucial in order to obtain a pulse duration around 8 ps, reducing the experimentally measured value of 25 ps by a factor of 3.

Then, motivated by recent experimental observations of high-contrast pulse-shaped localized structures in free-running ring QCLs such as Kerr optical solitons [35], we configure the ESMBEs for the description of a multimode ring QCL and we investigate the active HML in this configuration. We remark that no experimental practical realization of this technique in ring QCLs has been presented so far, so this analysis is aimed to outline if these systems could lead to improved pulse characteristics with respect to the FP case. In fact, a comprehensive comparative analysis between these two schemes is proposed, with the result that ring QCLs can actually ensure some progress in the realization of HML: High-power coherent sequences of pulses of duration 1.5 ps are numerically reproduced.

In Sec. II we introduce the ESMBEs for a THz QCL in both ring and FP configurations and we describe how the HML is implemented in the numerical model. Section III is dedicated to the numerical results for the FP cavity. In Sec. III A we analyze the role of the laser intrinsic parameters for a THz QCL in the achievement of HML, highlighting the points of difference with the fundamental active mode locking. In particular, we consider how the values of the α factor, carrier lifetime, and gain bandwidth impact the generation of coherent harmonic states when we perform HML. In Sec. III B we study the effect of the rf injection parameters, such as the modulation depth, the length of the modulated portion of the laser cavity, and the value of the current in the unmodulated section, with

particular focus on the analysis of contrast, duration, and peak power of the emitted pulses. Section IV is dedicated to the analysis of the configuration exploited in the experiment of Ref. [12]. Section V is about the numerical results for HML in ring QCLs, and a comparison with the FP case, based on a large stream of numerical simulations, is proposed. Section VI summarizes the work.

II. NUMERICAL MODEL

In order to study the dynamics of THz QCLs in the presence of harmonic modulation of the bias current, we exploit the ESMBEs. This model was first introduced in [34] for the description of a broadband ring QCL and then adapted to the Fabry-Pérot configuration in [17] for the description of the multimode dynamics of a mid-IR QCL. Recently, it was used in [16] for the study of a THz QCL in free-running operation and with active mode locking; in particular, the fundamental active mode locking was deeply analyzed and characterized in [16] and it was also shown that this model allows one to reproduce harmonic pulses when the modulation frequency is a multiple of the cavity FSR. This model is based on a phenomenological expression for the optical susceptibility of a semiconductor material and includes a linewidth enhancement factor, the dependence of the gain and refractive index on the density of carriers and frequency. In the FP case, it also encompasses the spatial hole burning (SHB), accounting for the dynamics of the carrier grating present in this configuration [7,8]. In this work, we study the HML in both ring and FP QCLs and therefore we introduce the ESMBEs for these two configurations.

A. Effective semiconductor Maxwell-Bloch equations for Fabry-Pérot QCLs

The full set of ESMBEs for FP QCLs adopted in this work is [16,17]

$$\frac{\partial E^+}{\partial z} + \frac{1}{v}\frac{\partial E^+}{\partial t} = -\frac{\alpha_L}{2}E^+ + gP_0^+, \tag{1}$$

$$-\frac{\partial E^-}{\partial z} + \frac{1}{v}\frac{\partial E^-}{\partial t} = -\frac{\alpha_L}{2}E^- + gP_0^-, \tag{2}$$

$$\frac{\partial P_0^+}{\partial t} = \pi\delta_{\text{hom}}(1+i\alpha)[-P_0^+ + if_0\varepsilon_0\varepsilon_b(1+i\alpha)(N_0E^+ + N_1^+E^-)], \tag{3}$$

$$\frac{\partial P_0^-}{\partial t} = \pi\delta_{\text{hom}}(1+i\alpha)[-P_0^- + if_0\varepsilon_0\varepsilon_b(1+i\alpha)(N_0E^- + N_1^-E^+)], \tag{4}$$

$$\frac{\partial N_0}{\partial t} = \frac{I}{eV} - \frac{N_0}{\tau_e} + \frac{i}{4\hbar}(E^{+*}P_0^+ + E^{-*}P_0^- - E^+P_0^{+*} - E^-P_0^{-*}), \tag{5}$$

$$\frac{\partial N_1^+}{\partial t} = -\frac{N_1^+}{\tau_e} + \frac{i}{4\hbar}(E^{-*}P_0^+ - E^+P_0^{-*}), \tag{6}$$

where $E^+(z,t)$ and $E^-(z,t)$ are the forward and backward envelopes, respectively, for the electric fields propagating inside the cavity; P_0^+ and P_0^- are the forward and backward
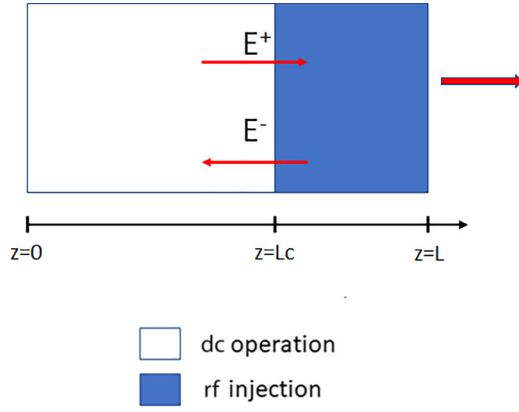
FIG. 1. Fabry-Pérot QCL configuration under rf injection. Here L_C is the length of the portion of the cavity with constant value of the bias current (dc operation). In the cavity section between $z = L_C$ and $z = L$ the rf injection is implemented and the bias current is a sinusoidal function of the time. The E^+ and E^- are the forward and backward fields, respectively, propagating inside the laser cavity.

polarization envelopes, respectively; N_0 is the density of carriers at zeroth order; N_1^+ and N_1^- are the first-order carrier density terms, which reproduce the carrier grating due to SHB occurring in the FP resonator furthermore; v is the group velocity; α_L is the waveguide loss; α is the linewidth enhancement factor; δ_{hom} is the full width at half maximum (FWHM) of the gain spectrum in the limit of the two-level system (i.e., where we consider $\alpha \ll 1$); f_0 is the differential gain; ε_0 is the vacuum dielectric permittivity; ε_b is the relative dielectric constant of the QCL active medium; I is the bias current; V is the volume of the QCL active medium; τ_e is the carrier lifetime; and the coefficient g is expressed by the equation

$$g = \frac{-i\omega_0 N_p \Gamma_c}{2\varepsilon_0 n_r c}, \tag{7}$$

where N_p is the number of stages of cascading structure, ω_0 is cold cavity frequency closest to the gain peak and it is used as a reference frequency, Γ_c is the optical confinement factor, c is the speed of light in vacuum, and n_r is the effective background refractive index of the medium. The boundary conditions for the FP cavity are

$$E^-(L, t) = \sqrt{R}E^+(L, t), \tag{8}$$

$$E^+(0, t) = \sqrt{R}E^-(0, t), \tag{9}$$

where R is the reflectivity of each facet of the QCL (we assume a symmetric configuration) and L is the cavity length. We want to implement a sinusoidal modulation of the bias current into a portion of the laser cavity, while the other portion is kept at the constant value of the current I_B. In fact, several theoretical and experimental studies about the QCL dynamics in the presence of rf injection have shown that this configuration enables the emission of a train of single-peaked high-contrast pulses [16,34,36–38]. This configuration is shown in Fig. 1. The bias current in the laser cavity is then expressed by

$$I(z, t) = \begin{cases} I_B & \text{if } 0 \leqslant z \leqslant L_C \\ I_0 + I_A \cos(2\pi\,\Omega_M t) & \text{if } L_C < z \leqslant L, \end{cases} \tag{10}$$
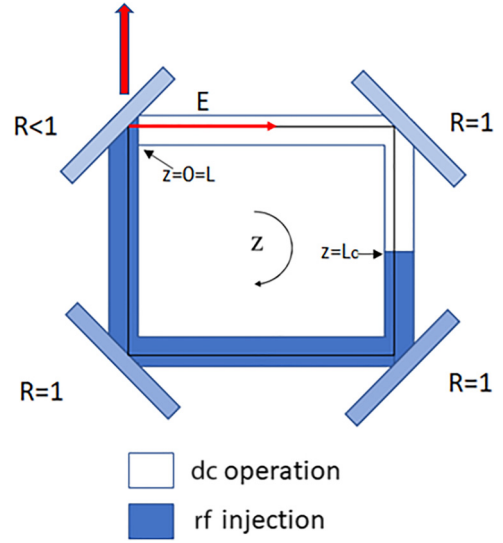

FIG. 2. QCL configuration under rf injection in a unidirectional ring cavity. We suppose three mirrors with reflectivity $R = 1$ and one mirror with reflectivity $R < 1$, which enables a portion of the light to escape from the resonator. Similar to the FP case, L_C is the length of the cavity section with constant value of the bias current (dc operation), while between $z = L_C$ and $z = L$ the bias current is modulated through rf injection.

where I_0 is the central value of the current, I_A is amplitude of the modulation, and Ω_M is the modulation frequency. Since we want to implement harmonic mode locking, the modulation frequency is a multiple n of the beat-note frequency, i.e., $\Omega_M = n f_{BN}$. Furthermore, the parameter $p = 1 - \frac{L_C}{L}$ represents the portion of the cavity where the rf injection is applied.

B. Effective semiconductor Maxwell-Bloch equations for ring QCLs

In addition to the FP resonator, we also study in this work the unidirectional ring QCL. A scheme of this configuration is shown in Fig. 2. The ESMBEs for this system can be retrieved starting from Eqs. (1)–(6), by assuming the hypotheses specific to the ring configuration. The unidirectionality implies that a single propagating field is considered, lacking the counterpropagating wave. Therefore, we impose

$$E^- = 0, \tag{11}$$

$$P_0^- = 0. \tag{12}$$

Furthermore, the absence of a standing wave in the cavity prevents the onset of the SHB, so we can eliminate the dynamical variables describing the carrier grating, imposing in Eqs. (1)–(6)

$$N_1^+ = 0, \tag{13}$$

$$N_1^- = 0. \tag{14}$$

Then we can remove the superscript +, so that the electric field is named E, and we can write the ESMBEs for a ring

TABLE I. Effective semiconductor Maxwell-Bloch equations' parameters.

Parameter	Value
length of the laser cavity	$L = 2$ mm
effective refractive index	$n_r = 3.6$
confinement factor	$\Gamma_c = 0.13$
mirror reflectivity	$R = 0.3$
differential gain	$f_0 = 7 \times 10^{-5}$ μm³
volume of the active region	$V = 3.6 \times 10^6$ μm³
number of stages	$N_p = 90$
central emission frequency	$\nu_0 = 3$ THz
waveguide losses	$\alpha_L = 3.8$ cm⁻¹

QCL:

$$\frac{\partial E}{\partial z} + \frac{1}{v}\frac{\partial E}{\partial t} = -\frac{\alpha_L}{2}E + gP_0, \tag{15}$$

$$\frac{\partial P_0}{\partial t} = \pi\delta_{\text{hom}}(1+i\alpha)[-P_0 + if_0\epsilon_0\epsilon_b(1+i\alpha)N_0E], \tag{16}$$

$$\frac{\partial N_0}{\partial t} = \frac{I}{eV} - \frac{N_0}{\tau_e} + \frac{i}{4\hbar}[E^*P_0 - EP_0^*]. \tag{17}$$

Finally, we complete the model with the boundary condition characteristic of this scheme (for further details, see [39]):

$$E(0,t) = \sqrt{R}E(L,t). \tag{18}$$

We remark that in [34], Eqs. (15)–(17) are coupled with a different boundary condition, with R replacing $\sqrt{R}$ in Eq. (18). This is due to the fact that a different configuration is analyzed. In fact, in [34] two mirrors with reflectivity $R < 1$ are considered in the ring scheme, while in Fig. 2 we assume a single region of coupling with the outside, associated with one reflection coefficient $R < 1$. We chose to study the scheme in Fig. 2 because it closely matches recently implemented experimental configurations for ring QCLs [7,8,35,40]. Since this work is aimed at investigating active HML, with the introduction of the rf injection in a portion of the QCL cavity (see Fig. 2), the bias current is expressed also in this case by Eq. (10).

III. NUMERICAL RESULTS FOR FABRY-PÉROT QCLS

This section is dedicated to the numerical results obtained by integrating the ESMBEs (1)–(6) with the boundary conditions (8) and (9) and the bias current expressed by Eq. (10), modulating at multiples of the round-trip frequency f_{BN}, which is extracted from a 1-μs-long free-running simulation with constant bias current I corresponding to the central value I_0 implemented in the rf injection. In all the performed simulations, the parameters shown in Table I are fixed and the value f_{BN} is about 20.8 GHz. The numerical method used for integration of the differential equations is based on a finite-difference scheme, discretizing in both time and space [17,41]. The same numerical method has been also used to integrate the ESMBEs in the ring configuration. The parameters of Table I have been chosen because they are typical of THz QCLs [8] and they allow us to correctly reproduce the multimode dynamics of these devices in free-running operation and with fundamental active mode locking (see [16]),

providing reasonable agreement with the experimental results available in the literature. The aim of the study proposed in this section is to highlight the role of the other parameters, which belong to two categories: the laser parameters, such as the α factor, carrier lifetime τ_e, and gain bandwidth, and the rf injection parameters, such as the current in the unmodulated portion, the modulation depth, and the length of modulated section of the cavity. We want to investigate how variations of these parameters influence the achievement of harmonic active mode-locked pulses and their characteristics. In particular, we characterize these power pulses by considering their duration, measured as the FWHM, and their contrast, defined by

$$S = \frac{P_{\text{max}} - P_{\text{min}}}{P_{\text{max}}}, \tag{19}$$

where P_{max} and P_{min} are the maximum and minimum values of the output power, respectively.

A. Effect of laser intrinsic parameters

We want to investigate the role of the laser parameters and in particular our analysis begins with the α factor. In [16] it has been shown that with the parameters of Table I and by considering $\tau_e = 5$ ps [7], $\delta_{\text{hom}} = 0.32$ THz, and $\alpha = -0.1$ [42] it is possible to obtain a sequence of harmonic pulses by modulating the bias current at a multiple of the BN frequency nf_{BN}, with a reduction of the contrast of these pulses with respect to the case $n = 1$, where contrast 1 is reported; furthermore, the obtained numerical optical spectrum for the case $n = 2$ resembles the experimental one reported in Ref. [12]. We remark that the exploited value of δ_{hom} is in agreement with typical values of gain bandwidth reported in the literature for a THz QCL [14,31]. In this case the value of the threshold current is $I_{\text{thr}} = 650$ mA. We recall that, since the actual gain bandwidth is given by the sum of δ_{hom} and an α-dependent term, an increase of α at fixed δ_{hom} implies an increase of the gain bandwidth. However, the α-dependent contribution is a minority compared to δ_{hom} (see [17]), and its increase with the linewidth enhancement factor (LEF) does not affect our statements. The exploited rf injection parameters are $I_A = 1.54I_{\text{thr}}$, $I_0 = 1.54I_{\text{thr}}$, and $p = 0.5$ (half cavity modulated). Corresponding to this set of parameters, we report lasing for $I_B > I_{B1} = 0.54I_{\text{thr}}$ and harmonic pulses for $I_B < I_{B2} = 0.69I_{\text{thr}}$, so for the simulation results shown in the following, we fix $I_B = 0.62I_{\text{thr}}$, at the center of the interval delimited by I_{B1} and I_{B2}, where the active HML occurs. More details about the role of I_B for the laser dynamics will be given in Sec. III B. An example of the experimental realization of active mode locking in a QCL with $I_B < I_{\text{thr}}$ was reported in Ref. [38]. Moreover, we would like to mention that the considered value of I_A has been chosen according to recently performed experiments in the presence of strong rf injection, which have shown that high values of the modulation depth favor the emission of a regular repetition of short pulses [43].

If we fix these values for all the parameters, but we vary α between -0.1 and 1.1, in steps of 0.3, we obtain the scenario shown in Fig. 3. In this figure we show the temporal evolution of the normalized output power (obtained by dividing the output power of each time trace by the maximum output power
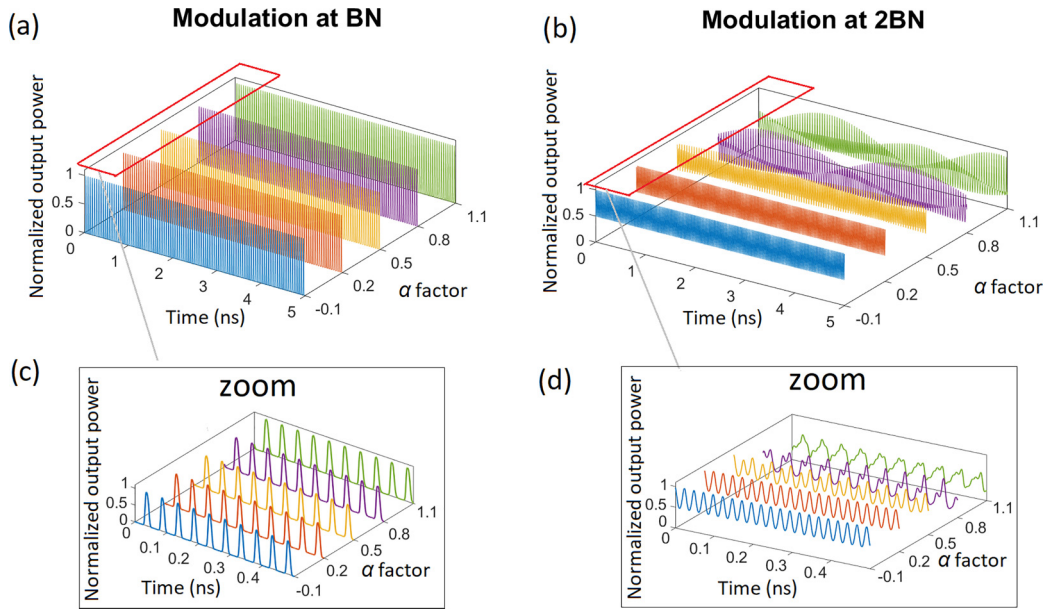
FIG. 3. Effect of the α factor on the laser dynamics under rf injection. The temporal evolution of the normalized output power is shown for different values of α: -0.1, 0.2, 0.5, 0.8, and 1.1. (a) and (c) Modulation at the BN frequency for a time interval of (a) 5 ns and a zoom in on (c) 0.5 ns. (b) and (d) Modulation at twice the BN frequency for a time interval of (b) 5 ns and a zoom in on (d) 0.5 ns. Simulations were performed for the parameters of Table I and $\tau_e = 5$ ps, $\delta_{\mathrm{hom}} = 0.32$ THz, $I_0 = 1.54 I_{\mathrm{thr}}$, $I_A = 1.54 I_{\mathrm{thr}}$, $I_B = 0.62 I_{\mathrm{thr}}$, and $p = 0.5$.

for that time trace) for different values of α, corresponding to fundamental and harmonic active mode locking. We display the normalized power instead of the power, because a change of α implies a change of the maximum power, so the comparison between the different waveforms appearing in each panel of Fig. 3 would be difficult and not efficient at all. From Figs. 3(a) and 3(c) we can observe that if the modulation frequency is f_{BN} (fundamental active mode locking), the pulses are stable with respect to changing α, and for all the cases we report a train of single-peaked power pulses with contrast 1. Conversely, if we implement HML at a modulation frequency $2f_{\mathrm{BN}}$ the situation drastically changes, as it can be observed in Figs. 3(b)–3(d). In this case, for the two lowest values of α we report regular harmonic pulses with contrast about 0.5, but then for higher values we observe the occurrence of power amplitude modulations on the nanosecond timescale, which implies a loss of coherence [Fig. 3(b)]. A zoom in on a time interval of 0.5 ns [Fig. 3(d)] shows that the increase of α causes a loss of the repetition frequency corresponding to $2f_{\mathrm{BN}}$ and the occurrence of dynamics on the fundamental round-trip frequency. We can explain this result by considering that the presence of a nonzero α factor in QCLs is one of the mechanisms which favors the occurrence of dense multimode dynamics. In fact, larger values of α correspond to an increase of the coupling between phase and amplitude of the electric field propagating in the FP resonator, leading to higher modal competition [7,27]. For this reason, an increase of this parameter beyond a certain threshold value which depends on the other laser parameters favors the occurrence of irregular unlocked regimes, as previously pointed out in a theoretical investigation on self-starting OFCs in these devices [17]. Then, also in the case of HML, for a high value of α the system is not able to support the propagation of coherent harmonic pulses, and multimode unlocked states characterized by

oscillations at the fundamental beat note are observable. This result suggests the coherence of the pulses in rf injected FP QCLs if favored by α lower than a threshold value and that therefore an experimental implementation of this technique can be more easily achieved in THz QCLs than in the mid-IR region, where higher values of this parameter are reported in the literature [7,8].

Let us explore how the value of the carrier lifetime influences the HML. In this case we fix all the parameters as in the previous analysis concerning the role of α and we vary the carrier lifetime τ_e between 1 and 13 ps in steps of 4 ps. In this analysis we set $\alpha = -0.1$. Since the variation of the τ_e implies also a variation of the laser threshold I_{thr}, in order to have consistency between the results we consider for all the performed simulations $I_0 = 1.54 I_{\mathrm{thr}}$, $I_A = 1.54 I_{\mathrm{thr}}$, and $I_B = 0.62 I_{\mathrm{thr}}$, where I_{thr} is different for each considered value of the carrier lifetime. Also in this case we decided to represent the normalized output power, because a change of the carrier lifetime implies a change of the maximum power, which would make a comparison between the set of time traces appearing on the same panel difficult. The results of our numerical investigation are shown in Fig. 4(a), where, as already mentioned, the normalized output power of the QCL under a modulation of the current at frequency $\Omega_M = 2f_{\mathrm{BN}}$ is presented. We note that an increase of τ_e causes a reduction of the contrast [note that in Fig. 4(a) the minimum of each curve increases with τ_e, while the maximum is fixed to 1 because of the normalization] and for the highest value $\tau_e = 13$ ps the regular repetition of harmonic pulses is lost, with two adjacent peaks corresponding to slightly different values of the power [see the inset in Fig. 4(a)]. If we calculate the FWHM of the pulses, we notice that for $\tau_e = 1$ ps we obtain a minimum pulse duration of 10.29 ps, while the FWHM increases by increasing the value of the carrier lifetime, as shown in
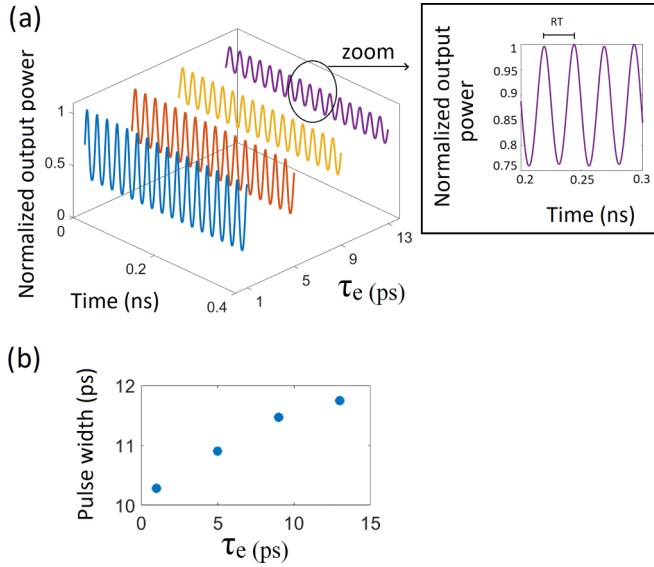
FIG. 4. Effect of the carrier lifetime τ_e on the laser dynamics under rf injection modulating at $2f_{BN}$. (a) Temporal evolution of the normalized output power for different values of τ_e: 1, 5, 9, and 13 ps. The inset shows a zoomed in view of the temporal power trace. Simulations were performed for the parameters of Table I and $\alpha = -0.1$, $\delta_{hom} = 0.32$ THz, $I_0 = 1.54I_{thr}$, $I_A = 1.54I_{thr}$, $I_B = 0.62I_{thr}$, and $p = 0.5$. Here RT denotes the round-trip time. (b) Calculated pulse width (FWHM) for the harmonic regimes presented in (a).

FIG. 5. Irregular dynamics in the temporal evolution of the power for bias current modulation at (a) f_{BN} and (b) $2f_{BN}$ for $\delta_{hom} = 0.80$ THz, $\alpha = -0.1$, $\tau_e = 5$ ps, $I_A = I_0 = 1.54I_{thr}$, $I_B = 0.62I_{thr}$, and $p = 0.5$. The other parameters are as in Table I.

Fig. 4(b). For the highest value $\tau_e = 13$ ps we report a pulse duration of 11.8 ps. Therefore, when the dynamics of the laser occurs on a faster timescale (lower carrier lifetime), also the system is able to support more efficiently a regular emission of a fast train of pulses and both the contrast and duration of these pulses are improved. Conversely, this effect vanishes if we consider the case $n = 1$ (modulation at the round-trip frequency): In this case we verified that the system is able to support a sequence of pulses with repetition frequency f_{BN} and contrast 1 independently of the considered value of the carrier lifetime. Furthermore, we remark that the values of pulse duration found have the same order of magnitude as the experimental pulse width reported in [12]. The experimental value (about 25 ps) is slightly higher than the duration of our simulated pulses, but this can be justified by considering that the laser cavity length exploited in the experiment is 6 mm, while we are considering a QCL 2 mm long: In the presence of a longer round-trip time, it is expected to have a longer pulse duration, but the orders of magnitude should be in agreement.

Finally, we want to analyze the effect of the gain bandwidth of the QCL active medium on the performance of the harmonic active mode locking. As shown in Figs. 3 and 4, for $\delta_{hom} = 0.32$ THz we report second-order harmonic pulses characterized by a duration of about 11 ps and a contrast around 0.5. We want to understand if these characteristics can be improved by increasing the gain bandwidth of the QCL. We fix then $\alpha = -0.1$ and $\tau_e = 5$ ps and we choose a higher value of the homogeneous gain bandwidth $\delta_{hom} = 0.80$ THz, which is comparable to the values of the gain bandwidth for a THz QCL reported in the literature, obtained by exploiting

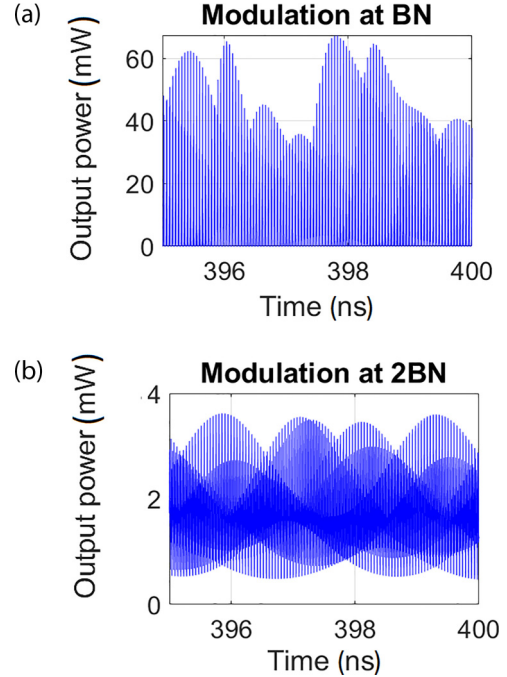particular QCL cavity designs, such as a planarized waveguide [44] or a multistack active region [45]. We remark that these solutions also allow us to obtain a gain profile wider than 1 THz. If we exploit the same rf injection parameters as in Figs. 3 and 4, we do not obtain a coherent sequence of pulses, but irregular regimes characterized by strong power oscillations, for both conventional [Fig. 5(a)] and harmonic [Fig. 5(b)] active mode locking. This is due to the fact that if we increase the gain bandwidth, the dynamical scenario for the free-running case changes, and for the value of the bias current $I = I_0 = 1.54I_{thr}$ we report an irregular regime corresponding to the new value of δ_{hom}. Therefore, the initial condition (the dynamics in free-running operation) plays a key role in the achievement of the coherence also in the presence of rf injection. We verify that coherent regimes are again obtained with active mode locking if we set I_0 inside the new comb region for the case $\delta_{hom} = 0.80$ THz. According to this, we choose as a working point for our analysis $I_0 = 1.08I_{thr}$, where the QCL emits a self-starting OFC regime, in order to be in the same condition as the previously discussed simulated case obtained for $\delta_{hom} = 0.32$ THz. If we choose $I_A = I_0 = 1.08I_{thr}$, $I_B = 0.92I_{thr}$, and $p = 0.67$, we obtain a train of pulses with contrast 1 modulating at $n = 2$ (blue curve in Fig. 6), which is compared with the power temporal evolution for the case $\delta_{hom} = 0.32$ THz (red curve). We note that the increase of the gain bandwidth implies the passage from a quasi-cw behavior to a set of high-contrast pulses, which is also accompanied by a reduction in the pulse width (12 ps in the $\delta_{hom} = 0.32$ THz case and 5 ps when $\delta_{hom} = 0.80$ THz). This is due to the fact that if the gain profile is larger, we have a decrease of the suppression ratio between the central
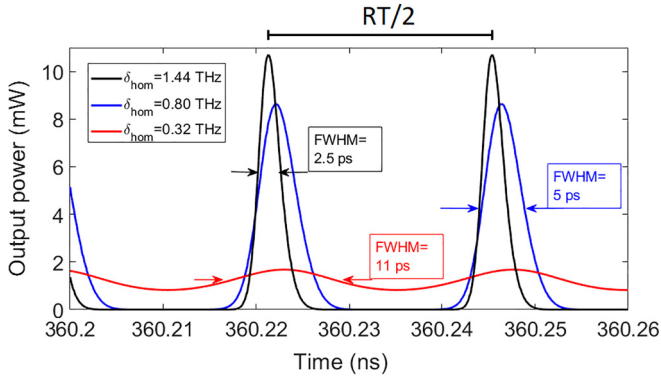
FIG. 6. Harmonic mode locking for different values of the gain bandwidth. The temporal evolution of the output power for a second-order HML is performed for $\delta_{\text{hom}} = 1.44$ THz (black curve), $\delta_{\text{hom}} = 0.80$ THz (blue curve), and $\delta_{\text{hom}} = 0.32$ THz (red curve), displaying a decrease in the pulse duration (measured as the FWHM) as the gain bandwidth increases.

mode and adjacent modes in the optical spectrum (which are displaced n times the FSR of the laser cavity) and therefore the side modes experience a gain closer to the central frequency. For this reason, the power does not exhibit a cw-like behavior, and higher contrast is achieved. If we increase the gain bandwidth to $\delta_{\text{hom}} = 1.44$ THz, we still obtain regular pulses with contrast 1 (black curve in Fig. 6) and we can shorten them to 2.5 ps, a value significantly lower than the experimental measurement reported in [12]. We mention that the duration of our simulated pulses is also lower than the minimum pulse width reported in fundamentally active mode-locked THz QCLs [46]. We understand, therefore, that while a reduction of the carrier lifetime implies a limited improvement in the pulse duration [see Fig. 4(b)], the gain bandwidth is the key parameter to be optimized in order to reach ultrashort pulses by using active mode locking in THz QCLs. New solutions for cavity design which provide a larger gain profile, such as multistack structures [45], are therefore essential to approach the picosecond limit. We finally remark that an increase of the gain bandwidth corresponds to a reduction of the polarization dephasing time τ_{d}, which is related to δ_{hom} through the equation $\delta_{\text{hom}} = \frac{1}{\pi \tau_{\text{d}}}$. Therefore, our results show that a shorter value of τ_{d} (larger gain bandwidth) enables the system to support the coherent formation of pulses of shorter duration. Furthermore, an increase of the gain bandwidth enables more optical modes to participate in the pulse formation, with a consequent reduction of the pulse width.

B. Effect of rf injection parameters

We are interested in discussing the effect of the rf injection parameters on the harmonic active mode locking. In particular, we want to consider the role of the modulation depth I_{A}, the dc I_{B} in the unmodulated section of the laser cavity, and the portion p where the rf injection is implemented.

Figure 7 shows an analysis of the pulses by modulating at $\Omega_{\text{M}} = 2f_{\text{BN}}$. In this simulation we swept I_{A} between $0.3I_{\text{thr}}$ and $1.54I_{\text{thr}}$ by keeping $I_{\text{B}} = 0.62I_{\text{thr}}$ and modulating half the cavity. Concerning the laser parameters, we use the values in Table I and $\delta_{\text{hom}} = 0.32$ THz, $\alpha = -0.1$, and $\tau_{\text{e}} = 5$ ps.
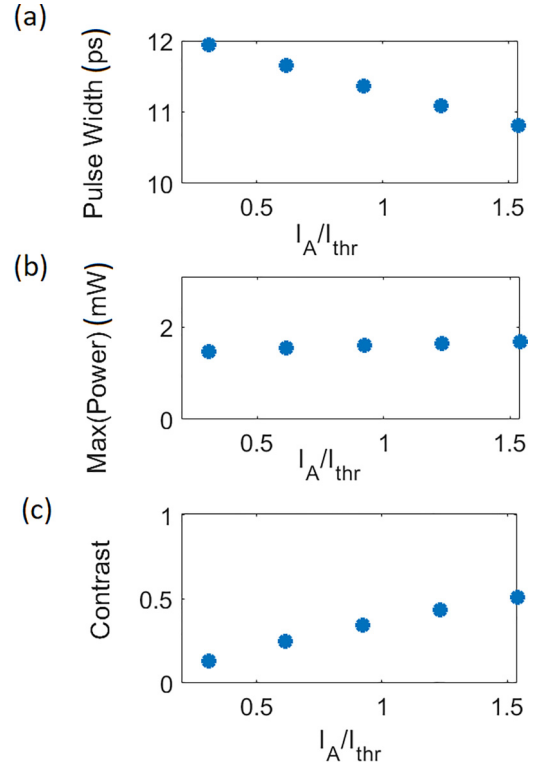

FIG. 7. Effect of the modulation depth I_{A} variation on active HML for the case $n = 2$: (a) pulse width, (b) power peak, and (c) contrast as a function of I_{A}. Here $\delta_{\text{hom}} = 0.32$ THz, $\alpha = -0.1$, $\tau_{\text{e}} = 5$ ps, $I_0 = 1.54I_{\text{thr}}$, $I_{\text{B}} = 0.62I_{\text{thr}}$, and $p = 0.5$. The other parameters are as in Table I.

These values of the QCL parameters are kept fixed for all the simulations presented in this section. We note that by increasing the modulation depth, the contrast [Fig. 7(c)] and the power [Fig. 7(b)] of the pulses are improved and also a decrease of the pulse width occurs [Fig. 7(a)]. Therefore, the modulation depth plays a key role in the improvement of the characteristics of the harmonic pulses, analogously to the scenario obtained for fundamental active mode locking [16].

In Fig. 8 we show how the second-order HML is affected by a variation of the current in the unmodulated portion of the cavity I_{B}, by fixing all the other parameters for laser and rf injection. We consider as a minimum value $I_{\text{B}} = 0.54I_{\text{thr}}$, since for lower values of I_{B} we do not have emitted power by implementing the rf injection with the exploited parameters, and as a maximum value $I_{\text{B}} = 0.69I_{\text{thr}}$, because for higher values we lose the coherence of the sequence of harmonic pulses. We note that maximum power and contrast are improved by increasing I_{B}, and the pulse duration slightly decreases, with values around 11 ps for all the performed simulations. These values have the same order of magnitude of the pulse duration of tens of picoseconds reported in the experimental demonstration of active HML [12]. However, our simulated pulses are slightly shorter than the experimental measurements of Ref. [12]. We explain this by noting that in the mentioned experiment the rf injection is implemented in the entire cavity of the QCL, a situation which drastically affects the contrast and duration of the obtained pulses, as shown in previous numerical studies [16,36]. Conversely, in our simulated
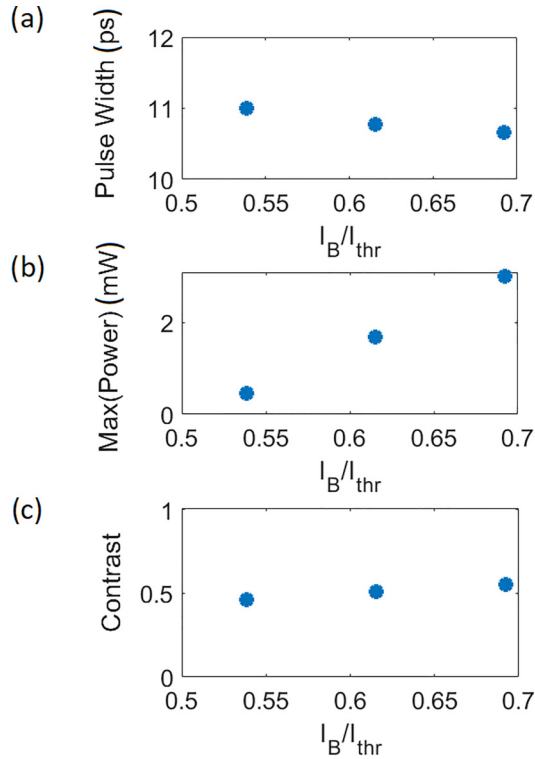
FIG. 8. Effect of the dc in the unmodulated section I_B on active HML for the case $n = 2$: (a) pulse width, (b) power peak, and (c) contrast as a function of I_A. Here $\delta_{hom} = 0.32$ THz, $\alpha = -0.1$, $\tau_e = 5$ ps, $I_A = I_0 = 1.54 I_{thr}$, and $p = 0.5$. The other parameters are as in Table I.
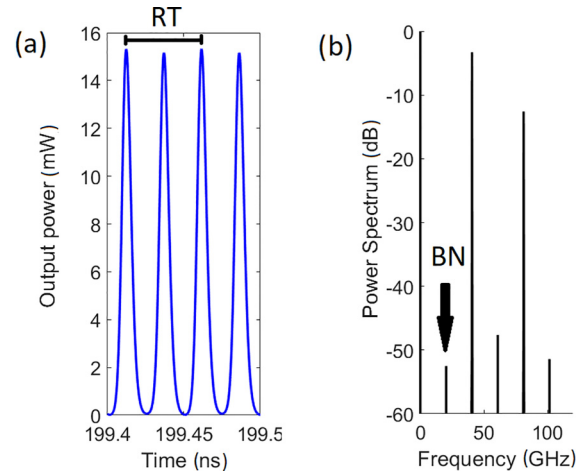

FIG. 9. Power as a function of the (a) time and (b) rf spectrum for the pulses obtained by modulating at twice the beat-note frequency, with $p = 0.6$. For this case $\delta_{hom} = 0.32$ THz, $\alpha = -0.1$, $\tau_e = 5$ ps, and $I_A = I_0 = 1.54 I_{thr}$. The other parameters are as in Table I.

configuration the rf injection is introduced in a portion of the QCL cavity and the value of I_B is chosen to minimize the pulse duration and maximize the contrast.

Finally, we consider different values for the portion of the modulated section, by keeping fixed $I_B = 0.62 I_{thr}$ and $I_A = 1.54 I_{thr}$, and we examine how the generation of harmonic pulses for the case $n = 2$ is affected by this parameter. For this parameter configuration, we find that when half the cavity is modulated ($p = 0.5$), a regular repetition of pulses is obtained, as previously shown, but by decreasing this value to 0.4, the emitted power vanishes, while increasing to 0.6 we lose the regular repetition of pulses each half-cavity round-trip (see Fig. 9). In this case, in fact, two adjacent pulses do not present the same value of the peak power [note that the peak of the second pulse is slightly lower than the first one in Fig. 9(a)] and consequentially a peak at the first beat-note frequency occurs in the rf spectrum [Fig. 9(b)], showing imperfect repetition at $2 f_{BN}$. We understand, therefore, that for typical laser parameters for THz QCLs and rf injection parameters, a value or an interval of values of p exists where a coherent emission of harmonic pulses is obtained (for the considered configuration, this value is 0.5).

IV. HARMONIC MODE LOCKING IN FABRY-PÉROT QCLS: DIRECT COMPARISON WITH EXPERIMENT

In this section we show the numerical results obtained by simulating the active HML in FP QCLs with the dynamical

model parameters retrieved from Ref. [12], where the only experimental demonstration of this technique is presented. In this way, we can draw a direct comparison with the experiment and we can more efficiently highlight possible solutions for the improvement of the pulse characteristics.

The ESMBE parameters are presented in Table II. We specify that the value of f_0 has been determined by imposing the constraint that the laser threshold is $I_{thr} = 900$ mA, as in the experiment (see Fig. S1 in the Supplemental Material of [12]). The value of polarization dephasing time $\tau_d = 0.6$ ps implies $\delta_{hom} = 0.53$ THz. The round-trip frequency is $f_{BN} = 6.94$ GHz. The only model parameter that is not provided in Ref. [12] is the α factor. We chose $\alpha = -0.1$, which is the value that allowed us to efficiently reproduce the multimode behavior of a THz QCL in [16] and which is typical of some THz QCL structures [8,42,47].

First, we integrate the ESMBEs implementing the rf injection in the entire cavity ($p = 1$), with modulation frequency $\Omega_M = 2 f_{BN}$, as in the experiment, obtaining the result shown in Fig. 10. Although we observe two pulses per round-trip, these present a slight difference in the peak value. The FWHM of each pulse is about 27 ps, in reasonable agreement with the experimentally found value of 25 ps [12]. We remark

TABLE II. ESMBE parameters retrieved from Ref. [12].

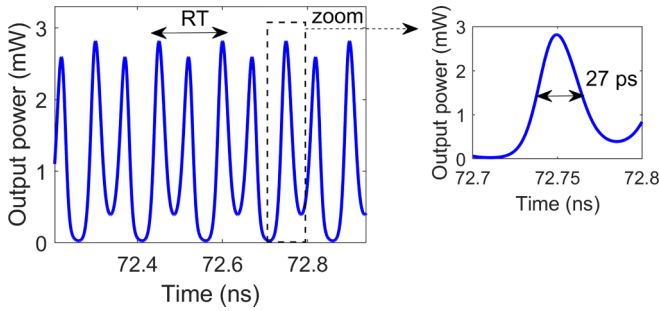| Parameter	Value
length of the laser cavity	$L = 6$ mm
effective refractive index	$n_r = 3.6$
confinement factor	$\Gamma_c = 1$
differential gain	$f_0 = 2.5 \times 10^{-8}$ μm³
volume of the active region	$V = 2.55 \times 10^4$ μm³
number of stages	$N_p = 180$
central emission frequency	$\nu_0 = 3$ THz
waveguide losses	$\alpha_L = 16$ cm⁻¹
carrier lifetime	$\tau_e = 10$ ps
polarization dephasing time	$\tau_d = 0.6$ ps

FIG. 10. Simulated temporal evolution of the output power under active HML, with the parameters of Table II and $\alpha = -0.1$, $\Omega_M = 2f_{BN}$, $p = 1$, and $I_0 = I_A = 1.05I_{thr}$. The inset shows a zoomed-in view of one of the simulated pulses. The width of this pulse is 27 ps.

that, based on the theoretical analysis reported in [16] and on numerical investigations performed by using conventional Maxwell-Bloch equations (see, e.g., [36]), it is not possible to reproduce a coherent sequence of high-contrast pulses if the rf injection is implemented in the entire cavity. Thus, it is necessary to introduce an unmodulated section, as shown in Fig. 1. For this reason, we consider different values of p and I_B and we test our simulator in this configuration with the parameters of Table II. We assume the same bias condition of Fig. 10, $I_0 = I_A = 1.05I_{thr}$, and we consider $n = 2$, as in the experiment. The results are presented in the map of Fig. 11. We notice that, in agreement with our results of Sec. III B, for some combinations of I_B and p no emitted power is reported (blue circles). In particular, the concomitance of a small modulated section and a low value of the bias current in the unmodulated portion of the cavity implies a power loss in the device, with a consequent decrease of the emitted power. For this reason, for some pairs (p and I_B) the emitted power vanishes. For the

case $I_B = I_{thr}$ and $p = 0.5$ (black circle) we report an unlocked regime, characterized by two pulses with different peak power in each round-trip, similar to the result shown in Fig. 10, with an additional superimposed amplitude modulation. In the red circles, which correspond to coherent sequences of harmonic pulses, the characteristics of these numerically reproduced pulses are reported. Contrast $S = 1$ is found for all the locked cases. We notice that at a fixed value of p, the peak power relevantly grows by increasing the value of I_B, while the pulse width is around 8–9 ps for all the considered cases. This constitutes an improvement with respect to the results obtained with the entire cavity modulated ($p = 1$), where a FWHM of 25 ps is reported in the experiment, and pulses with a FWHM of 27 ps are numerically reproduced (Fig. 10). Considering that the cavity round-trip time is 144 ps, the introduction of an unmodulated section provides a considerable reduction of the pulse duration from 17.4% to 6% of the cavity round-trip time. These results show that the importance of an unmodulated portion in the QCL cavity is twofold: On the one hand, it provides an increase of the degree of locking of the pulses; on the other hand, it is an efficient way to decrease the pulse duration.

V. NUMERICAL RESULTS FOR RING QCLS

In this section we present the results obtained by numerical integration of the ESMBEs for a ring QCL (15)–(17) with the boundary condition (18) and bias current expressed by Eq. (10). Since the active HML has not been implemented in ring QCLs so far and no theoretical or numerical analysis is currently present in the literature in this regard, our study is aimed to understand if this configuration can be efficiently exploited for the implementation of HML, drawing a comparative analysis with the FP case. Moreover, we want to identify
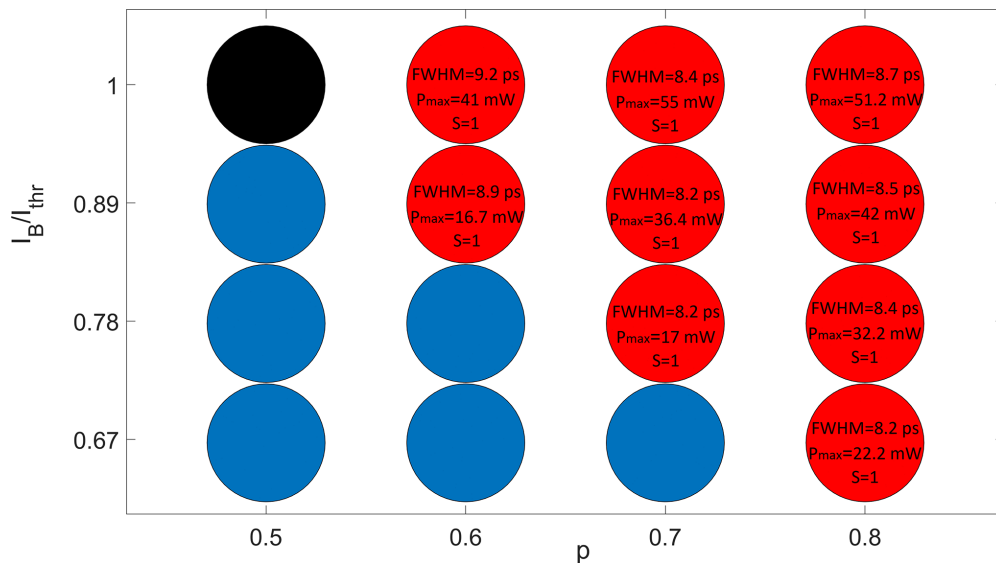

FIG. 11. Map showing the characteristics of the harmonic pulses obtained by simulating active HML for different values of p (portion of the cavity where the rf injection is applied) and I_B (current in the unmodulated portion of the cavity). The ESMBE parameters are as in Table II, in addition to $\alpha = -0.1$, $\Omega_M = 2f_{BN}$, and $I_0 = I_A = 1.05I_{thr}$. Blue circles denote no power emitted, the black circle is an unlocked regime, and red circles show a coherent sequence of harmonic pulses. In each red circle we report the FWHM, maximum power, and contrast of such pulses. The values of p are chosen between 0.5 and 0.8 in steps of 0.1, while the values of I_B are between $0.67I_{thr}$ and I_{thr} with steps of $0.11I_{thr}$.
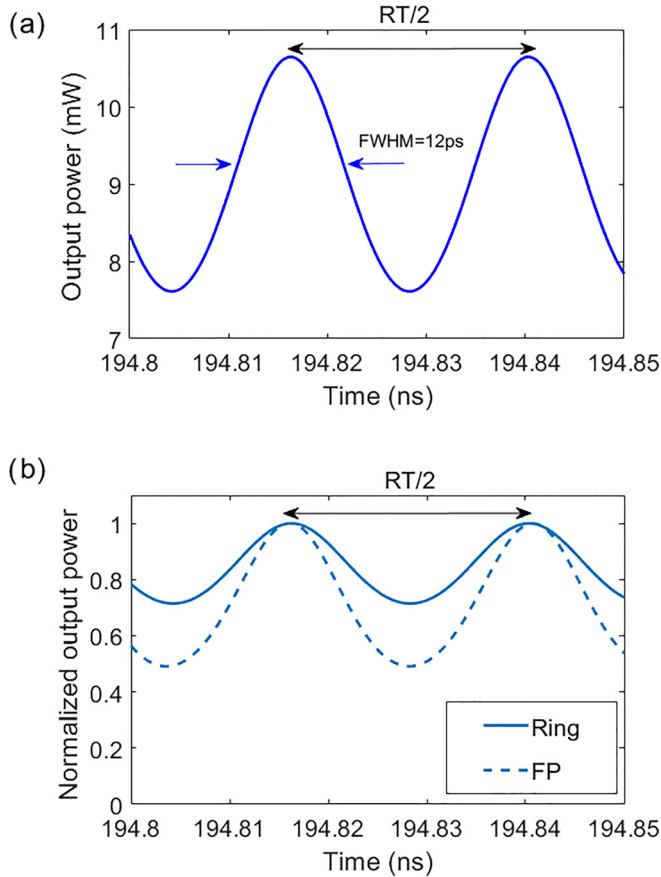
FIG. 12. (a) Temporal evolution of the output power for a simulated ring QCL, with the parameters of Table I and $L = 4$ mm, $\alpha = -0.1$, $\delta_{\rm hom} = 0.32$ THz, $I_A = I_0 = 1.54 I_{\rm thr}$, $p = 0.5$, $I_B = 0.62 I_{\rm thr}$, and $\Omega_M = 2 f_{\rm BN}$; the FWHM of each simulated pulse is 12 ps. (b) Normalized output power versus time obtained simulating the HML in ring (solid line) and FP (dashed line) QCL, exploiting the same set of parameters for the two cases (except L, which is double in the ring case, to match the FSR of the two configurations); the parameters are the ones specified in (a).

a convenient parameter configuration for the generation of harmonic short pulses by rf injection. First, we adopt the same parameters exploited for the study of a FP QCL presented in Table I, in order to draw a first comparison between the two configurations. The only exception is L, which we set to a value of 4 mm instead of 2 mm to have the same FSR of the FP case. We choose $\alpha = -0.1$ and $\delta_{\rm hom} = 0.32$ THz, as in Sec. III. We preliminarily study the free-running operation of the ring laser with these parameters, reporting $I_{\rm thr} = 475$ mA. We sweep the driving current I between $I_{\rm thr}$ and $3 I_{\rm thr}$, reporting single-mode emission for every I. We relate the single-mode behavior of the laser to the concurrence of a considered low value of the α factor and the absence of SHB in the unidirectional ring configuration. In fact, these two are the main physical mechanisms triggering the multimode dynamics near threshold in QCLs [8].

At this point, we introduce a modulation of the bias current [Eq. (10)] for the study of the HML. To enable a comparison with the results obtained for the FP case, we set $I_A = I_0 = 1.54 I_{\rm thr}$, $p = 0.5$, and $\Omega_M = 2 f_{\rm BN}$, as in Sec. III. In Fig. 12(a)
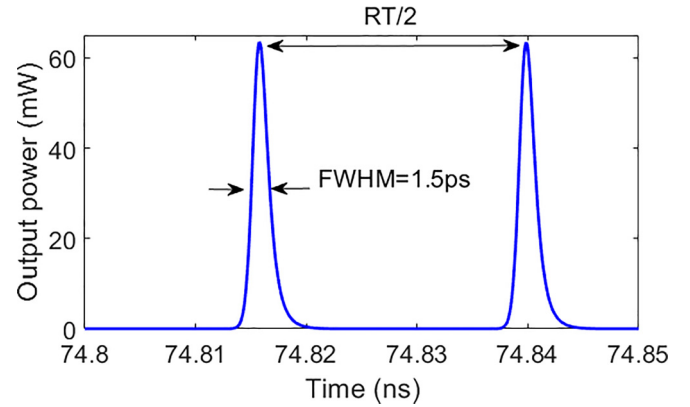

FIG. 13. Ultrashort pulses with FWHM $= 1.5$ ps in a ring QCL, with $\alpha = 1$, $\delta_{\rm hom} = 1.28$ THz, and the other parameters as in Fig. 12(a).

we show the obtained ring harmonics pulses (power versus time) and in Fig. 12(b) we display on the same plot FP and ring second-order harmonic pulses (normalized output power versus time) for this parameter set. We specify that the normalized solid curve in Fig. 12(b) (ring) corresponds to the unnormalized plot of Fig. 12(b), while the dashed plot (FP) refers to the red curve in Fig. 6, characterized by pulses of duration 11 ps. We notice that the FP configuration provides higher contrast ($S = 0.5$) than the ring one ($S = 0.3$) and a slightly shorter pulse duration (11 ps instead of 12 ps). We relate this to the different free-running behavior occurring in the two systems (as mentioned, the ring is single mode, while the FP emits a fundamental frequency comb for $I = 1.54 I_{\rm thr}$). Since α has the same value in both cases, we conclude that the absence of the SHB is the key factor to prevent the onset of intrinsic multimode dynamics in the ring for this parameter configuration, affecting in turn the characteristics of the pulses of Fig. 12.

At this point, we are interested in comparing the HML in ring and FP configurations when both systems develop free-running multimode dynamics. This can be induced by increasing the α factor or the gain bandwidth. We consider, for example, a ring QCL with $\alpha = 1$ and $\delta_{\rm hom} = 1.28$ THz, keeping all the other parameters fixed as in Fig. 12(a). In this case we are able to reproduce a sequence of high-contrast ($S = 1$) harmonic pulses of duration 1.5 ps (see Fig. 13), which is a value lower than the shortest one obtained in the FP case (FWHM of 2.5 ps, black curve in Fig. 6).

In order to better highlight the role of the α factor and the gain or dispersion bandwidth in affecting the figure of merit of the harmonic pulses and at the same time draw up a comprehensive comparison between ring and FP schemes, we simulate the HML in both configurations for $\alpha = 0.5, 1, 1.5$ and values of $\delta_{\rm hom}$ between 0.32 and 1.6 THz in steps of 0.32 THz. For each pair ($\delta_{\rm hom}$ and α) we scan the central value of the modulated bias current I_0 between $I_{\rm thr}$ and $2 I_{\rm thr}$ in steps of $0.1 I_{\rm thr}$, with $I_A = I_0$ and other rf injection parameters as in Fig. 12. The ESMBE parameters are as in Table I, with cavity length $L = 4$ mm for the ring resonator and $L = 2$ mm for the FP one, in order to have the same FSR for the two cavities. We remark that, except for L, the same parameters
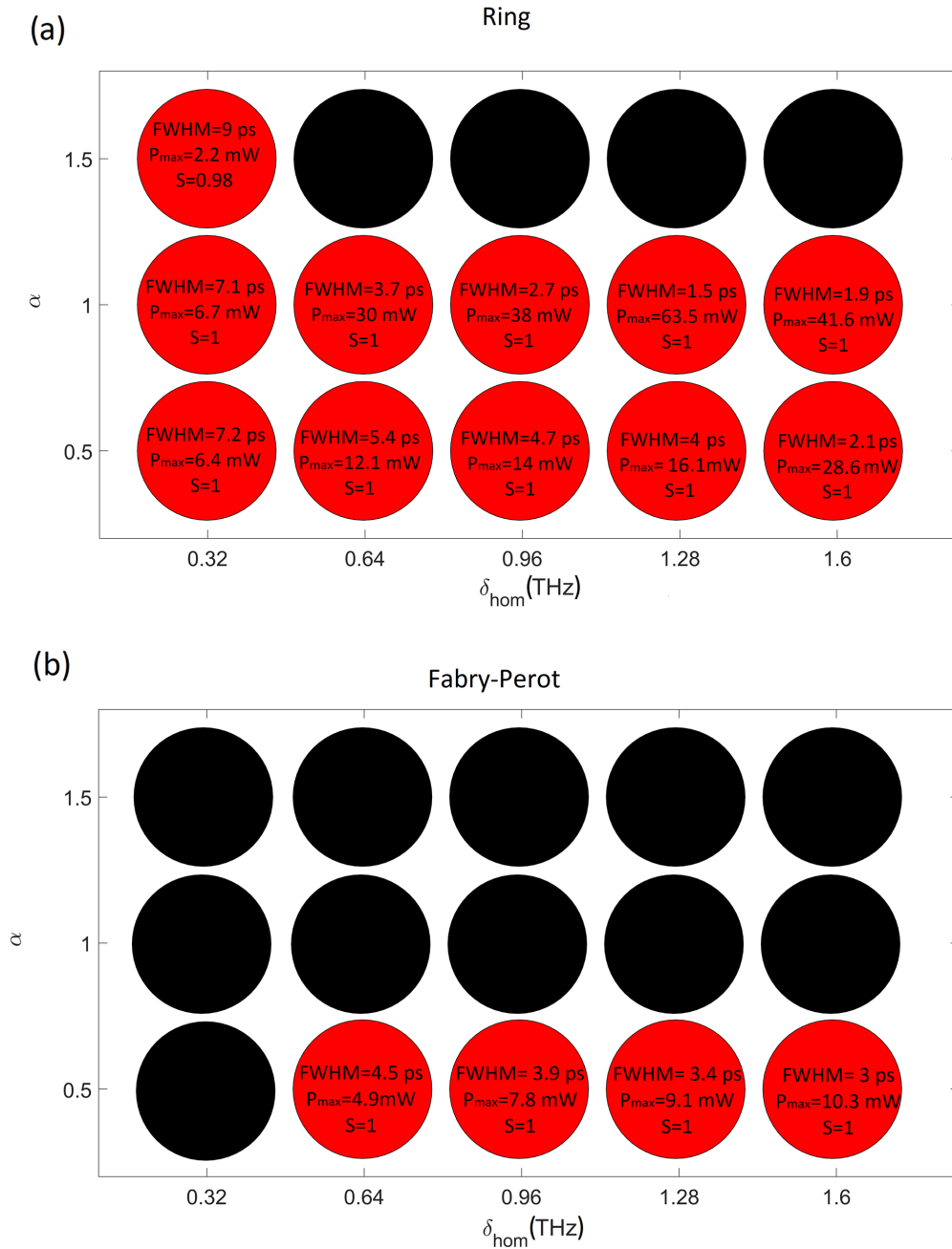
FIG. 14. Analysis of harmonic pulses upon variation of α and δ_{hom} for (a) ring and (b) FP QCLs. Black circles indicate that no locked states could be found upon scanning the central value of the modulated current I_0 between I_{thr} and $2I_{thr}$ in steps of $0.1 I_{thr}$; red circles indicate that coherent sequences of pulses are observed in the simulations. In the red circles, the FHWM, maximum power P_{max}, and contrast S of such pulses are reported. Here $I_A = I_0$ is assumed for all the simulations. The parameter values of Table I have been exploited for both configurations; the cavity length is $L = 4$ mm for the ring resonator and $L = 2$ mm for the FP cavity.

are used for the simulation of both FP and ring QCLs. The results are summarized in Fig. 14(a) (ring) and Fig. 14(b) (FP), where we represent the couple (δ_{hom} and α) with a red circle if coherent pulses are reported and with a black circle if no locked states are observed. In each red circle we report the FWHM, maximum power P_{max}, and contrast S of the simulated harmonic pulses.

We first analyze the results related to the ring configuration, presented in Fig. 14(a). We observe coherent regimes for the majority of the considered pairs (δ_{hom} and α), with unlocked states reported for $\alpha = 1.5$ (the highest considered value) and δ_{hom} between 0.64 and 1.6 THz. We explain this by observing that if α increases, the modal competition inside the QCL cavity is enhanced, due to the higher coupling between the phase and amplitude of the electric field, promoting the occurrence of irregular dynamical regimes. A similar behavior was reported in [17], regarding the case of self-starting frequency combs in mid-IR QCLs. Furthermore, we observe that for a fixed value of δ_{hom}, if α is increased from 0.5 to 1, the pulse duration decreases and the peak power of the pulses grows.

This is due to the fact that higher α favors the multimode operation of the laser [16] so that more cavity modes are involved in the pulse formation, implying higher power and shorter width. The only exception to this trend is found for $\delta_{\text{hom}} = 0.32$ THz, where for $\alpha = 1.5$ we report a larger pulse width (FWHM of 9 ps) than for $\alpha = 1$ (FWHM of 7.1 ps). We impute this to the procedure followed to implement the HML in our numerical investigation. In fact, for each pair (δ_{hom} and α) and each value of I_0, we preliminarily run a simulation of the laser in free-running operation with bias current $I = I_0$ in order to retrieve f_{BN}; then the extracted f_{BN} is used to calculate the modulation frequency $\Omega_{\text{M}} = 2f_{\text{BN}}$, exploited for the simulation of the active HML. In the case of $\delta_{\text{hom}} = 0.32$ THz and $\alpha = 1.5$, the free-running operation of the ring laser is an irregular regime, so a broad line is observed in the power spectrum, which in turn affects the accuracy in the estimation of the BN frequency f_{BN}. This causes a deterioration in the performance of active mode locking, leading to larger and less powerful pulses than in the resonant case (see [16,36]).

If α is fixed and δ_{hom} is increased, we observe a reduction of the pulse duration as a general trend, similarly to the results of Fig. 6 for the FP cavity. In the case of the ring resonator, however, we are able to obtain a FWHM of less than 2 ps for $\alpha = 1$ and δ_{hom} values of 1.28 and 1.6 THz. This suggests that ring QCLs could constitute a valid potential alternative to the FP ones, for achieving the generation of subpicosecond pulses in the THz spectral range, a long-standing goal for the research in this field of study [48]. We remark that the unidirectional ring resonator intrinsically supports the propagation of high-contrast pulsed structures in QCLs, with the emission of solitons and Turing rolls in free-running operation and with optical injection [8,22,23,35,40]. The values of α considered in Fig. 14 are in agreement with the ones used in recent theoretical studies where the mentioned high-contrast localized structures have been reproduced [22,40]. About the general trend of FWHM reduction upon an increase of δ_{hom}, we mention that a single exception is found going from $\delta_{\text{hom}} = 1.28$ to 1.6 THz at fixed $\alpha = 1$. We justify this anomaly by noticing that the shortest coherent pulses (FWHM of 1.9 ps) for the case $\delta_{\text{hom}} = 1.6$ THz have been found corresponding to $I_0 = 1.1 I_{\text{thr}}$ (for higher values of I_0 only unlocked states have been observed under rf injection), while for $\delta_{\text{hom}} = 1.28$ THz the narrowest pulses (FWHM of 1.5 ps) correspond to a higher central value of the bias current ($I_0 = 1.5 I_{\text{thr}}$). Thus, the higher value of δ_{hom} does not automatically imply a lower FWHM: For a larger gain bandwidth the narrowest coherent pulses can be observed for a low value of the bias current, so the number of modes participating in the pulse formation is lower, with a consequent broader FHWM.

We examine now Fig. 14(b), which summarizes the results for the FP cavity obtained with the same parameters as in Fig. 14(a). First, we notice that for $\alpha = 1$ and 1.5 no locked pulses are found, while in the ring case we report sequences of coherent harmonic regimes for these two values of the LEF. This suggests that in the FP laser the simultaneous presence of SHB (and therefore of a carrier grating) and modal competition provided by the α factor prevents the occurrence of locked states for high values of the LEF. Not only is this behavior valid for active mode-locked regimes, but it has also

been found by comparing the formation of self-starting QCL frequency combs in these two configurations [17,18,34].

Then we observe that the minimum pulse duration reported in Fig. 14(b) is 3 ps, close to the value 2.5 ps found in Sec. III with another parameter set. However, it is quite larger than the lowest value reported in Fig. 14(a) for the ring QCL (1.5 ps). Thus, the absence of SHB allows us to have coherent states for a higher α factor, the resulting key property of unidirectional ring QCLs which enables the generation of ultrashort pulses with a duration of about 1 ps.

This comparative analysis suggests that an experimental implementation of the HML by adopting ring QCLs instead of the FP ones could entail a significant improvement in the performance of this method, paving the way for the generation of subpicosecond pulses in the THz range.

VI. CONCLUSION

We proposed a numerical study of the dynamics of a THz QCL under HML. The first part of the work was dedicated to the FP configuration, which we investigated to analyze the role of laser intrinsic parameters and rf injection in the formation and the characteristics of the harmonic pulses. We showed that an increase of the α factor implies a progressive loss of coherence of the QCL dynamics when we modulate at a multiple of the BN frequency, due to the increased modal competition associated with the enhanced coupling between the amplitude and phase of the electric field in the laser cavity. Furthermore, the dynamics of the laser for different values of the carrier lifetime was investigated. We found that an increase of this parameter implies a reduction of the contrast, and for the highest value considered also the coherence was lost, showing that an intrinsically faster dynamics of the QCL supports more efficiently the propagation of harmonic pulses. The maximization of the contrast and the minimization of the pulse duration occur for a carrier lifetime of 1–5 ps.

However, the key parameter to be optimized for the achievement of ultrashort pulses is the gain bandwidth. In fact, we showed that by considering a value of the gain bandwidth of 1.44 THz, pulses with a duration of 2.5 ps were numerically reproduced [12]. Therefore, this analysis suggests that the realization of optimized cavity designs allowing for a large gain profile, such as multistack active regions, is a key point for the generation of pulses with duration approaching and possibly beating the picosecond limit.

Then we analyzed the impact of the driving current modulation parameters on the characteristics of the pulses, developing a procedure for a maximization of contrast and peak power and the achievement of shorter duration. With regard to the effect of rf injection parameters, the main outcome is that a high value of the modulation depth favors an improvement of the pulse characteristics, which also improve if the length of the modulated portion of the cavity and the dc in the unmodulated section are chosen in a specific interval defined by the other laser parameters.

Furthermore, we performed a direct comparison between numerical results and the only HML experiment reported in the literature, by adopting the parameters extracted from Ref. [12]. We found that a relevant improvement in the pulse characteristics could be achieved by introducing an

unmodulated section in the QCL cavity. In this case, in fact, we could predict pulses three times shorter than in the experiment.

Finally, we proposed a theoretical study of the HML in ring QCLs, motivated by the fact that these devices are intrinsically able to support the propagation of high-contrast pulse-shaped structures, such as cavity solitons and Turing rolls. We made a comparison with the FP configuration, showing that the unidirectional nature of ring resonators leads to the possibility

to reach pulse widths lower than in FP QCLs, with a reported minimum value of 1.5 ps.

[1] J. Faist, *Quantum Cascade Lasers* (Oxford University Press, Oxford, 2013).

[2] J. Faist, F. Capasso, D. L. Sivco, C. Sirtori, A. L. Hutchinson, and A. Y. Cho, Quantum cascade laser, Science **264**, 553 (1994).

[3] R. Köhler, A. Tredicucci, F. Beltram, H. E. Beere, E. H. Linfield, A. G. Davies, D. A. Ritchie, R. C. Iotti, and F. Rossi, Terahertz semiconductor-heterostructure laser, Nature (London) **417**, 156 (2002).

[4] S. S. Dhillon, M. S. Vitiello, E. H. Linfield, A. G. Davies, M. C. Hoffmann, J. Booske, C. Paoloni, M. Gensch, P. Weightman, G. P. Williams, E. Castro-Camus, D. R. S. Cumming, F. Simoens, I. Escorcia-Carranza, J. Grant, S. Lucyszyn, M. Kuwata-Gonokami, K. Konishi, M. Koch, C. A. Schmuttenmaer *et al.*, The 2017 terahertz science and technology roadmap, J. Phys. D **50**, 043001 (2017).

[5] D. Burghoff, T.-Y. Kao, N. Han, C. W. I. Chan, X. Cai, Y. Yang, D. J. Hayton, J.-R. Gao, J. L. Reno, and Q. Hu, Terahertz laser frequency combs, Nat. Photon. **8**, 462 (2014).

[6] J. Faist, G. Villares, G. Scalari, M. Rösch, C. Bonzon, A. Hugi, and M. Beck, Quantum cascade laser frequency combs, Nanophotonics **5**, 272 (2016).

[7] M. Piccardo and F. Capasso, Laser frequency combs with fast gain recovery: Physics and applications, Laser Photon. Rev. **16**, 2100403 (2022).

[8] C. Silvestri, X. Qi, T. Taimre, K. Bertling, and A. D. Rakić, Frequency combs in quantum cascade lasers: An overview of modeling and experiments, APL Photon. **8**, 020902 (2023).

[9] X. Qi, G. Agnew, T. Taimre, S. Han, Y. L. Lim, K. Bertling, A. Demić, P. Dean, D. Indjin, and A. D. Rakić, Laser feedback interferometry in multi-mode terahertz quantum cascade lasers, Opt. Express **28**, 14246 (2020).

[10] A. Forrer, Y. Wang, M. Beck, A. Belyanin, J. Faist, and G. Scalari, *Conference on Lasers and Electro-Optics Europe and European Quantum Electronics Conference, Munich, 2021* (IEEE, Piscataway, 2021).

[11] A. Forrer, Y. Wang, M. Beck, A. Belyanin, J. Faist, and G. Scalari, Self-starting harmonic comb emission in THz quantum cascade lasers, Appl. Phys. Lett. **118**, 131112 (2021).

[12] F. Wang, V. Pistore, M. Riesch, H. Nong, P.-B. Vigneron, R. Colombelli, O. Parillaud, J. Mangeney, J. Tignon, C. Jirauschek, and S. S. Dhillon, Ultrafast response of harmonic modelocked THz lasers, Light Sci. Appl. **9**, 51 (2020).

[13] S. S. Dhillon, in *Novel In-Plane Semiconductor Lasers XX*, edited by A. A. Belyanin and P. M. Smowton, SPIE Conf. Proc. No. 11705 (SPIE, Bellingham, 2021).

[14] H. Li, W. Wan, Z. Li, J. C. Cao, S. Lepillet, J.-F. Lampin, K. Froberger, L. Columbo, M. Brambilla, and S. Barbieri, Real-time multimode dynamics of terahertz quantum cascade lasers via intracavity self-detection: Observation of self mode-locked population pulsations, Opt. Express **30**, 3215 (2022).

[15] N. Opačak and B. Schwarz, Theory of Frequency-Modulated Combs in Lasers with Spatial Hole Burning, Dispersion, and Kerr Nonlinearity, Phys. Rev. Lett. **123**, 243902 (2019).

[16] C. Silvestri, X. Qi, T. Taimre, and A. D. Rakić, Multimode dynamics of terahertz quantum cascade lasers: Spontaneous and actively induced generation of dense and harmonic coherent regimes, Phys. Rev. A **106**, 053526 (2022).

[17] C. Silvestri, L. L. Columbo, M. Brambilla, and M. Gioannini, Coherent multi-mode dynamics in a quantum cascade laser: Amplitude- and frequency-modulated optical frequency combs, Opt. Express **28**, 23846 (2020).

[18] C. Silvestri, L. L. Columbo, M. Brambilla, and M. Gioannini, Dynamics of Optical Frequency Combs in Ring and Fabry-Perot Quantum Cascade Lasers, *2021 Conference on Lasers and Electro-Optics Europe & European Quantum Electronics Conference (CLEO/Europe-EQEC)* (Munich, Germany, 2021), p. 1.

[19] C. Jirauschek and T. Kubis, Modeling techniques for quantum cascade lasers, Appl. Phys. Rev. **1**, 011307 (2014).

[20] D. Burghoff, Unraveling the origin of frequency modulated combs using active cavity mean-field theory, Optica **7**, 1781 (2020).

[21] L. Humbard and D. Burghoff, Analytical theory of frequency-modulated combs: Generalized mean-field theory, complex cavities, and harmonic states, Opt. Express **30**, 5376 (2022).

[22] L. Columbo, M. Piccardo, F. Prati, L. A. Lugiato, M. Brambilla, A. Gatti, C. Silvestri, M. Gioannini, N. Opačak, B. Schwarz, and F. Capasso, Unifying Frequency Combs in Active and Passive Cavities: Temporal Solitons in Externally Driven Ring Lasers, Phys. Rev. Lett. **126**, 173903 (2021).

[23] F. Prati, M. Brambilla, M. Piccardo, L. L. Columbo, C. Silvestri, M. Gioannini, A. Gatti, L. A. Lugiato, and F. Capasso, Soliton dynamics of ring quantum cascade lasers with injected signal, Nanophotonics **10**, 195 (2021).

[24] F. Prati, L. Lugiato, A. Gatti, L. Columbo, C. Silvestri, M. Gioannini, M. Brambilla, M. Piccardo, and F. Capasso, Global and localised temporal structures in driven ring quantum cascade lasers, Chaos, Soliton. Fract. **153**, 111537 (2021).

[25] A. Hugi, G. Villares, H. C. L. Stéphane Blaser, and J. Faist, Mid-infrared frequency comb based on a quantum cascade laser, Nature (London) **492**, 229 (2012).

[26] F. Cappelli, L. Consolino, G. Campo, I. Galli, D. Mazzotti, A. Campa, M. Siciliani de Cumis, P. Cancio Pastor, R. Eramo, M. Rösch, M. Beck, G. Scalari, J. Faist, P. De Natale, and S. Bartalini, Retrieval of phase relation and emission profile of quantum cascade laser frequency combs, Nat. Photon. **13**, 562 (2019).

[27] M. Singleton, P. Jouy, M. Beck, and J. Faist, Evidence of linear chirp in mid-infrared quantum cascade lasers, Optica **5**, 948 (2018).

[28] D. Burghoff, Y. Yang, D. J. Hayton, J.-R. Gao, J. L. Reno, and Q. Hu, Evaluating the coherence and time-domain profile of quantum cascade laser frequency combs, Opt. Express **23**, 1190 (2015).

[29] P. Gellie, S. Barbieri, J.-F. Lampin, P. Filloux, C. Manquest, C. Sirtori, I. Sagnes, S. P. Khanna, E. H. Linfield, A. G. Davies, H. Beere, and D. Ritchie, Injection-locking of terahertz quantum cascade lasers up to 35 GHz using RF amplitude modulation, Opt. Express **18**, 20799 (2010).

[30] S. Barbieri, M. Ravaro, P. Gellie, G. Santarelli, C. Manquest, C. Sirtori, S. P. Khanna, E. H. Linfield, and A. G. Davies, Coherent sampling of active mode-locked terahertz quantum cascade lasers and frequency synthesis, Nat. Photon. **5**, 306 (2011).

[31] H. Li, P. Laffaille, D. Gacemi, M. Apfel, C. Sirtori, J. Leonardon, G. Santarelli, M. Rösch, G. Scalari, M. Beck, J. Faist, W. Hänsel, R. Holzwarth, and S. Barbieri, Dynamics of ultra-broadband terahertz quantum cascade lasers for comb operation, Opt. Express **23**, 33270 (2015).

[32] G. Scalari, A. Forrer, U. Senica, S. Cibella, G. Torrioli, P. Micheletti, M. Beck, and J. Faist, in *Novel In-Plane Semiconductor Lasers XXI*, edited by A. A. Belyanin and P. M. Smowton, SPIE Conf. Proc. No. 12021 (SPIE, Bellingham, 2022).

[33] D. Bachmann, M. Rösch, M. J. Süess, M. Beck, K. Unterrainer, J. Darmo, J. Faist, and G. Scalari, Short pulse generation and mode control of broadband terahertz quantum cascade lasers, Optica **3**, 1087 (2016).

[34] L. L. Columbo, S. Barbieri, C. Sirtori, and M. Brambilla, Dynamics of a broad-band quantum cascade laser: From chaos to coherent dynamics and mode-locking, Opt. Express **26**, 2829 (2018).

[35] B. Meng, M. Singleton, J. Hillbrand, M. Franckié, M. Beck, and J. Faist, Dissipative Kerr solitons in semiconductor ring lasers, Nat. Photon. **16**, 142 (2022).

[36] Y. Wang and A. Belyanin, Active mode-locking of mid-infrared quantum cascade lasers with short gain recovery time, Opt. Express **23**, 4173 (2015).

[37] C. Y. Wang, L. Kuznetsova, V. M. Gkortsas, L. Diehl, F. X. Kärtner, M. A. Belkin, A. Belyanin, X. Li, D. Ham, H. Schneider, P. Grant, C. Y. Song, S. Haffouz, Z. R. Wasilewski, H. C. Liu, and F. Capasso, Mode-locked pulses from

mid-infrared quantum cascade lasers, Opt. Express **17**, 12929 (2009).

[38] J. Hillbrand, N. Opačak, M. Piccardo, H. Schneider, G. Strasser, F. Capasso, and B. Schwarz, Mode-locked short pulses from an 8 μm wavelength semiconductor laser, Nat. Commun. **11**, 5788 (2020).

[39] C. Silvestri, Theory and modelization of quantum cascade laser dynamics: Comb formation, field structures and feedback-based imaging, Ph.D. thesis, Politecnico di Torino, 2022.

[40] M. Jaidl, N. Opačak, M. A. Kainz, S. Schönhuber, D. Theiner, B. Limbacher, M. Beiser, M. Giparakis, A. M. Andrews, G. Strasser, B. Schwarz, J. Darmo, and K. Unterrainer, Comb operation in terahertz quantum cascade ring lasers, Optica **8**, 780 (2021).

[41] P. Bardella, L. L. Columbo, and M. Gioannini, Self-generation of optical frequency comb in single section quantum dot Fabry-Perot lasers: A theoretical study, Opt. Express **25**, 26234 (2017).

[42] Y. Leng Lim, P. Dean, M. Nikolić, R. Kliese, S. P. Khanna, M. Lachab, A. Valavanis, D. Indjin, Z. Ikonić, P. Harrison, E. H. Linfield, A. Giles Davies, S. J. Wilson, and A. D. Rakić, Demonstration of a self-mixing displacement sensor based on terahertz quantum cascade lasers, Appl. Phys. Lett. **99**, 081108 (2011).

[43] A. Forrer, L. Bosco, M. Beck, J. Faist, and G. Scalari, RF injection of THz QCL combs at 80 K emitting over 700 GHz spectral bandwidth, Photonics **7**, 9 (2020).

[44] U. Senica, A. Forrer, T. Olariu, P. Micheletti, S. Cibella, G. Torrioli, M. Beck, J. Faist, and G. Scalari, Planarized THz quantum cascade lasers for broadband coherent photonics, Light Sci. Appl. **11**, 347 (2022).

[45] D. Bachmann, M. Rösch, C. Deutsch, M. Krall, G. Scalari, M. Beck, J. Faist, K. Unterrainer, and J. Darmo, Spectral gain profile of a multi-stack terahertz quantum cascade laser, Appl. Phys. Lett. **105**, 181118 (2014).

[46] F. Wang, H. Nong, T. Fobbe, V. Pistore, S. Houver, S. Markmann, N. Jukam, M. Amanti, C. Sirtori, S. Moumdji, R. Colombelli, L. Li, E. Linfield, G. Davies, J. Mangeney, J. Tignon, and S. Dhillon, Short terahertz pulse generation from a dispersion compensated mode-locked semiconductor laser, Laser Photon. Rev. **11**, 1700013 (2017).

[47] R. P. Green, J.-H. Xu, L. Mahler, A. Tredicucci, F. Beltram, G. Giuliani, H. E. Beere, and D. A. Ritchie, Linewidth enhancement factor of terahertz quantum cascade lasers, Appl. Phys. Lett. **92**, 071106 (2008).

[48] F. Wang, X. Qi, Z. Chen, M. Razeghi, and S. Dhillon, Ultrafast pulse generation from quantum cascade lasers, Micromachines **13**, 2063 (2022).